ADVANCING EARTH AND SPACE SCIENCES

JGR Atmospheres

RESEARCH ARTICLE
10.1029/2024JD041784

Global Temperature Dependency of Biogenic HCHO Columns Observed From Space: Interpretation of TROPOMI Results Using GEOS-Chem Model

Xicheng Li[1], Lei Zhu[1,2,3], Isabelle De Smedt[4], Wenfu Sun[4], Yuyang Chen[1], Lei Shu[5], Dakang Wang[6], Song Liu[1], Dongchuan Pu[1], Juan Li[1], Xiaoxing Zuo[1], Weitao Fu[1], Yali Li[1], Peng Zhang[1], Zhuoxian Yan[1], Tzung-May Fu[1,2,3], Huizhong Shen[1,2,3], Chen Wang[1,2,3], Jianhuai Ye[1,2,3], and Xin Yang[1,2,3]

[1]School of Environmental Science and Engineering, Southern University of Science and Technology, Shenzhen, China, [2]Guangdong Provincial Observation and Research Station for Coastal Atmosphere and Climate of the Greater Bay Area, Shenzhen, China, [3]Shenzhen Key Laboratory of Precision Measurement and Early Warning Technology for Urban Environmental Health Risks, School of Environmental Science and Engineering, Southern University of Science and Technology, Shenzhen, China, [4]Division of Atmospheric Composition, Royal Belgian Institute for Space Aeronomy, Brussels, Belgium, [5]School of Geographical Sciences, Fujian Normal University, Fuzhou, China, [6]School of Geography and Remote Sensing, Guangzhou University, Guangzhou, China

Key Points:

- Temperature (T-) dependency of biogenic HCHO columns varies substantially across plant functional types (PFTs)
- The GEOS-Chem model with the MEGAN module implemented primarily interprets the T-dependency of HCHO columns at the PFT level
- The T-dependency of biogenic volatile organic compound (BVOC) emissions mainly accounts for that of HCHO columns in Broadleaf Evergreen Tropical Trees and Warm C4 Grass regions

Supporting Information:

Supporting Information may be found in the online version of this article.

Correspondence to:

L. Zhu,
zhul3@sustech.edu.cn

Citation:

Li, X., Zhu, L., De Smedt, I., Sun, W., Chen, Y., Shu, L., et al. (2024). Global temperature dependency of biogenic HCHO columns observed from space: Interpretation of TROPOMI results using GEOS-Chem model. *Journal of Geophysical Research: Atmospheres*, *129*, e2024JD041784. https://doi.org/10.1029/2024JD041784

Received 12 JUN 2024
Accepted 21 OCT 2024

Abstract Temperature is the principal driver of global atmospheric formaldehyde (HCHO) and its primary oxidation precursor biogenic volatile organic compounds (BVOCs). We revisit such a temperature (T-) dependency globally, leveraging TROPOMI HCHO column data. We find substantial variations in the T-dependency of biogenic HCHO across plant functional types (PFTs), with the highest over Broadleaf Evergreen Tropical Trees (doubling every 6.0 K ± 4.1 K) and lowest over Arctic C3 Grass (doubling every 30.8 K ± 9.6 K). The GEOS-Chem model interprets HCHO columns' T-dependency at the PFT level ($r = 0.87$), with a 16% discrepancy on average. The discrepancy can be explained by BVOC emissions T-dependency for Broadleaf Evergreen Tropical Trees and Warm C4 Grass and can be attributed to the insensitivity of HCHO columns to BVOC emissions for other PFTs. Our findings underscore a potentially magnified variation of BVOC emissions by GEOS-Chem and MEGAN therein, particularly in regions experiencing greater temperature variations.

Plain Language Summary We use remote sensing data from an up-to-date monitor to examine the temperature (T-) dependency of biogenic formaldehyde (HCHO), a proxy of a series of volatile organic gases released by plants, in a global manner. We find that the effect of temperature on HCHO varies significantly between different types of plants, with tropical evergreen trees showing the most sensitivity to temperature and Arctic grasses showing the least. The GEOS-Chem, a state-of-the-art chemical transport model, interprets such temperature sensitivity among plants with nonnegligible discrepancies. The sensitivity of volatile organic gases released by plants to temperature explains the sensitivity of HCHO to temperature for some plants, such as tropical evergreen trees and warm-season grasses.

1. Introduction

Biogenic volatile organic compounds (BVOCs) account for 90% of the total VOC emissions (Guenther et al., 1995), significantly affecting atmospheric chemistry and air quality via the secondary production of tropospheric ozone (Hofzumahaus et al., 2009; Pacifico et al., 2012) and organic aerosols (Janssen et al., 2013; Kroll et al., 2006). Isoprene is the most abundant BVOC species (Arneth et al., 2008; Guenther et al., 2012; Sindelarova et al., 2014) with emissions highly dependent on temperature, as reported in North and South America, North Europe, and Africa (Alves et al., 2018; Bourtsoukidis et al., 2024; Harley et al., 2003, 2004; Langford et al., 2017; Rhew et al., 2017; Stoy et al., 2021). Previous studies have documented satellite HCHO columns as a proxy of BVOC emissions and demonstrated that regional HCHO columns depend on temperature variations (Duncan et al., 2009; Kaiser et al., 2018; Palmer et al., 2006; Zhu et al., 2014). Here, we examine the global distribution of such a temperature (T-) dependency in biogenic-dominated regions for the first time using high-resolution observations from the TROPOspheric Monitoring Instrument (TROPOMI) (Veefkind et al., 2012). We interpret such T-dependency using MEGAN implemented in GEOS-Chem model.

BVOC emissions are sensitive to temperature accompanied by other environmental factors, including plant function types (PFTs) (Arneth et al., 2011; Bonan et al., 2002; Bourtsoukidis et al., 2024; Misztal et al., 2011, 2016), photosynthesis (Litvak et al., 1996; Van Meeningen et al., 2017; Wang et al., 2022), soil moisture (Naimark et al., 2021; Zheng et al., 2017), and CO_2 concentrations (Garcia et al., 2019; Heald et al., 2009; Tai et al., 2013). Although isoprene emission flux has been measured among plant species and environmental conditions globally ranging from 0.1 to 93 mg C m^{-2} day^{-1} (Cao et al., 2021), site measurements lack representativeness of the region. Different choices of model parameters as well as the limited understanding of those environmental factors can give results with a factor of four errors for one region (Wu et al., 2020). Therefore, accurately quantifying BVOC emissions globally is highly challenging.

As a highly yielded product from BVOC oxidations, HCHO has an atmospheric lifetime of a few hours, making it a proxy of local and global BVOC emissions (Barkley et al., 2013; Curci et al., 2010; Millet et al., 2006, 2008; Palmer et al., 2003, 2006; Shim et al., 2005; Wolfe et al., 2016; Zhu et al., 2014; Zhu, & Mickley et al., 2017). Temperature is the most influential driver of satellite HCHO column variations (Abbot et al., 2003; Duncan et al., 2009; Guenther et al., 2006; Naimark et al., 2021; Palmer et al., 2006; Steiner et al., 2010; Zhu et al., 2014; Zhu, & Mickley et al., 2017), likely related to the rate-limiting process of BVOC (especially isoprene) synthase enzymatic reaction in plants (Monson et al., 1992; Rasulov et al., 2010; Sharkey et al., 2007). HCHO columns have been reported to be exponentially dependent on temperature in regions with abundant BVOC emissions (Ryan, & Rhodes et al., 2020; Ryan, & Silver et al., 2020; Zhu et al., 2014). This study explores such dependency globally using a 5-year monthly TROPOMI HCHO columns over the biogenic-dominated areas and interprets the dependency with the state-of-the-art MEGAN module v2.1 (Guenther et al., 2012) implemented in the GEOS-Chem model (v12.9.3) (Bey et al., 2001).

2. TROPOMI HCHO Columns

HCHO is detectable from space as a vertical column density (VCD), retrieved from the backscattered ultraviolet radiance from 325 to 360 nm (Chance et al., 2000). TROPOMI, on board the Copernicus Sentinel-5 Precursor satellite (S5P) launched in October 2017, is a nadir viewing shortwave spectrometer instrument using passive remote sensing techniques to attain its objectives at 13:30 daily local time. Among the available products, TROPOMI provides retrievals at a finer spatial resolution of 7.0×3.5 km^2 (upgraded to 5.5×3.5 km^2 since August 2019) and signal-to-noise ratio (De Smedt et al., 2018, 2021), with the algorithm inherited and updated from its predecessors, including the Global Ozone Monitoring Experiment (GOME) (De Smedt et al., 2008), SCanning Imaging Absorption spectroMeter for Atmospheric ChartograpHY (SCIAMACHY) (De Smedt et al., 2008; Wittrock et al., 2006), Ozone Monitoring Instrument (OMI) (De Smedt et al., 2015), GOME-2A (De Smedt et al., 2012), and GOME-2B (De Smedt et al., 2015).

Validation exercises with ground-based Multi-AXis Differential Optical Absorption Spectroscopy (MAX-DOAS) (Chan et al., 2020; De Smedt et al., 2021; Ryan et al., 2023) and Fourier-Transform InfraRed (FTIR) (Vigouroux et al., 2020) instruments show high temporal ($r = 0.71$ to 0.88) and spatial ($r = 0.85$ to 0.91) correlations, confirming the validity of TROPOMI HCHO product. Therefore, TROPOMI HCHO product has been widely used in constraining both biogenic and anthropogenic VOC emissions (Jin et al., 2023; Zhao et al., 2022; Zuo et al., 2023) and the implication for ozone levels (Goldberg et al., 2022; Li et al., 2021).

We select June 2018–May 2023 TROPOMI level 2 overpassing daily pixels with (a) quality assurance values greater than 0.5, (b) cloud fraction less than 0.3, (c) solar zenith angle less than 60°, and (d) snow-ice-free flag. We re-grid and oversample the resulted pixels onto the $0.5° \times 0.5°$ ($\sim 50 \times 50$ km^2) monthly grids, considering a trade-off between ensuring sufficient pixels and reasonable computing speed, built on our Oversampling method (Pu et al., 2022; Sun et al., 2021; Zhu et al., 2014; Zhu, & Jacob et al., 2017; Zhu, & Mickley et al., 2017; Zuo et al., 2023). The re-gridding method allows a precise allocation of pixels by area weight, and the oversampling method allows strict filtering criteria and increases the spatial signal-to-noise ratio by sacrificing temporal resolution. Further analysis is limited to grids where biogenic emissions are the main driver of HCHO columns (79% of the total continental grids), as determined from GEOS-Chem sensitivity simulations to the sources from biogenic, anthropogenic, and biomass burning (Text S1 and Figure S1 in Supporting Information S1).

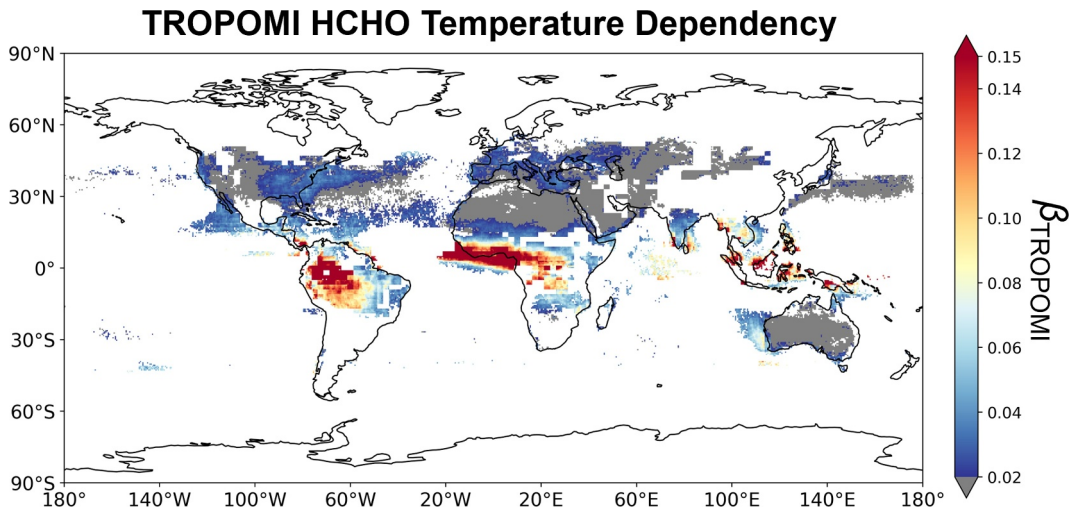

Figure 1. Global temperature (T-) dependency of TROPOMI HCHO columns. $\beta_{TROPOMI}$ (unit: ln (10^{15} molecules cm^{-2}) K^{-1}) is the TROPOMI HCHO T-dependency, fitted with $\Omega_{TROPOMI} = \exp(\alpha_{TROPOMI} + \beta_{TROPOMI}\, T + \varepsilon)$ at each $0.5° \times 0.5°$ grid, where $\Omega_{TROPOMI}$ is a vector of monthly oversampled TROPOMI HCHO columns and T is a vector of the monthly mean 2-m temperature (>285 K) correspond to $\Omega_{TROPOM.}$ $\alpha_{TROPOMI}$ is the fitting baseline and ε is the fitting residual. Only showing are biogenic-dominated grids (Figure S1 in Supporting Information S1) with significant $\beta_{TROPOMI}$ (p-value <0.05) and high determination coefficients ($R^2 > 0.5$, Figure S2 in Supporting Information S1). Low T-dependency regions (<0.02), such as the barren Sahara, are in gray and excluded from further analysis.

3. Global Temperature Dependency of TROPOMI HCHO Columns

We assign each oversampled HCHO column grid with a MERRA-2 surface temperature (T2M) according to its location and time. Here, we use air temperature as an indicator of leaf temperature, as they are positively and linearly correlated (Blonder & Michaletz, 2018; Fauset et al., 2018; Still et al., 2022). To quantify the T-dependency of HCHO columns, we apply the ordinary least squares regression to fit the exponential relationship between HCHO columns and temperature in each grid.

$$\Omega = \exp(\alpha + \beta T + \varepsilon) \tag{1}$$

where Ω (molecules cm^{-2}) denotes a vector of monthly HCHO columns. T (K) is a vector of T2M with a baseline of 285 K. We discard the records with T2M lower than 285 K from the fitting, considering enzyme activity in BVOC productions is suppressed at low temperatures (Lehning et al., 1999), and isoprene emissions increase markedly at around 12°C (Goldstein et al., 1998). β, in the unit of ln (molecules cm^{-2}) K^{-1}, quantifies the T-dependency of HCHO columns. α is the baseline after the logarithm, and ε is the fitting residuals. We focus on biogenic-dominated grids (Figure S1 in Supporting Information S1) with significant β (p-value <0.05) and temperature explaining the majority of HCHO variations ($R^2 > 0.5$) (Figure S2 in Supporting Information S1). Low T-dependency regions, such as barren and background areas, are filtered out from further analysis by a criterion of 0.02, the value over the Sahara Desert. Around 75% and 79% of the standardized residual from fitting grids over the research regions are considered normal and independent, respectively, indicating that the T-dependency fitting captures the main patterns and sources of variation. We admit that radiation flux (Zhang et al., 2019) and leaf phenology (Surl et al., 2018) also jointly influence the HCHO variation with temperature in specific regions, such as Mid Amazon and North India.

As shown in Figure 1, the T-dependency of TROPOMI HCHO columns ($\beta_{TROPOMI}$) has a more pronounced response over land. This highlights the dominant contribution of isoprene from terrestrial plants (Arnold et al., 2009; Guenther et al., 2006, 2012; Palmer & Shaw, 2005), especially in Southeast US (McKinney et al., 2011; Pressley et al., 2005; Stoy et al., 2021) and Amazon (Alves et al., 2023; Wei et al., 2018). $\beta_{TROPOMI}$ decreases along the latitudes, with the maximum in the Amazon, tropical rainforests along the equator in Africa, and Southeast Asia, consistent with reported in situ isoprene emission hot spots (Jaars et al., 2016; Langford et al., 2022; Misztal et al., 2011). Such T-dependency appears to be a seasonal variation: summertime and rainy

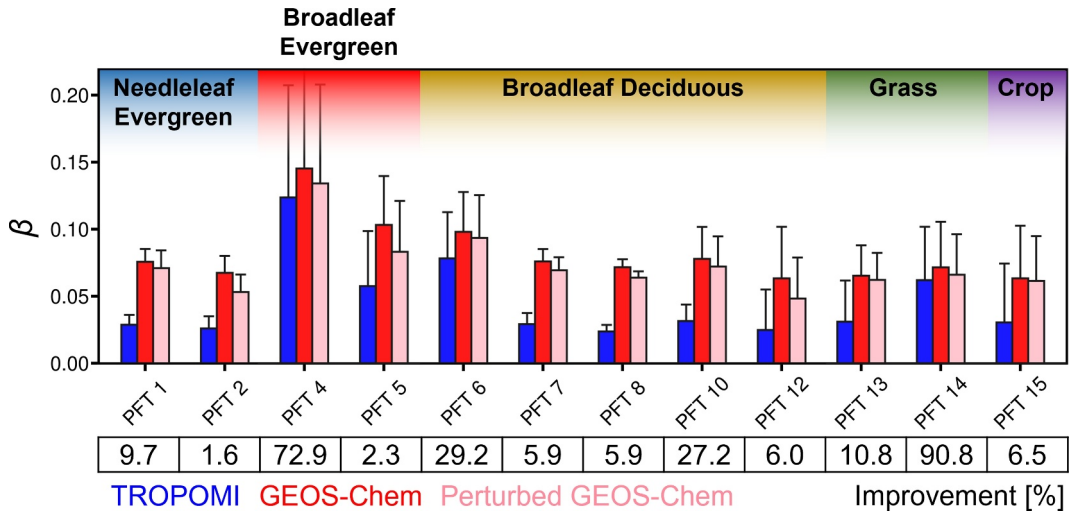

Figure 2. Temperature (T-) dependency of TROPOMI (β_{TROPOMI}, blue), GEOS-Chem ($\beta_{\text{GEOS-Chem}}$, red), and perturbed GEOS-Chem ($\beta'_{\text{GEOS-Chem}}$, pink) HCHO columns across plant functional types (PFTs). The error bar is the standard deviation of the β for grids with the same PFT, demonstrating the variations in T-dependency within the PFT. GEOS-Chem results are corrected with TROPOMI averaging kernels (Text S2 in Supporting Information S1). The perturbed GEOS-Chem incorporates β_{TROPOMI} into the temperature activity factor (γ'_T; Equation 2). Percentages quantify changes from $\beta_{\text{GEOS-Chem}}$ to $\beta'_{\text{GEOS-Chem}}$, relative to β_{TROPOMI}. PFTs are labeled in order: 1 Needleleaf Evergreen Temperate Tree, 2 Needleleaf Evergreen Boreal Tree, 4 Broadleaf Evergreen Tropical Tree, 5 Broadleaf Evergreen Temperate Tree, 6 Broadleaf Deciduous Tropical Tree, 7 Broadleaf Deciduous Temperate Tree, 8 Broadleaf Deciduous Boreal Tree, 10 Broadleaf Deciduous Temperate Shrub, 12 Arctic C3 Grass, 13 Cool C3 Grass, 14 Warm C4 Grass, and 15 Crop.

seasons have a notably higher T-dependency compared to wintertime and dry seasons (Figure S3 in Supporting Information S1).

We further examine mean β_{TROPOMI} across PFTs on land (Figure S4 in Supporting Information S1), by starting with the Broadleaf Evergreen Tropical Tree (PFT 4) dominated regions, such as Amazon, the equator of Africa, and Southeast Asia, where isoprene and monoterpene emissions contribute to 88% and 83% of the global total (Sindelarova et al., 2014), respectively. We see from Figure 2 that β_{TROPOMI} is the highest (0.12 ± 0.07) for PFT 4, translating to that HCHO columns would double every 6.0 K ± 4.1 K. This aligns with isoprene emissions variations measured in Amazon (Jardine et al., 2014, 2016; Pétron et al., 2001). β_{TROPOMI} is the lowest for the Broadleaf Deciduous Boreal Tree (doubling every 27.6 K ± 4.8 K). As summarized in Table S1 of Supporting Information S1, the doubling temperature ranges from 9.2 to 30.8 K for other PFTs, enveloping values from previous observation-based studies (Duncan et al., 2009; Pressley et al., 2005). The standard deviation is notable for some PFTs, such as Broadleaf Evergreen Trees (PFT 4 and 5) and Grasses (PFT 13 and 14), indicating a large variation in T-dependency within those PFT groups. Nevertheless, most of the T-dependency PFTs pairs are significantly different (Tukey pairwise post hoc test) except for 4 Broadleaf Deciduous species (PFT 7, 8, 10, and 12), acknowledging that the joint influence of latitudinal distribution on PFTs and T-dependency is non-negligible, especially in the lower latitudes (Figure S5 in Supporting Information S1).

Figure 1 also shows significant T-dependencies over the ocean, including off the coast around the Caribbean, the Gulf of Guinea, the ocean near Southeast India, the ocean near Western Australia, and coastal areas of the southeast US. We examine potential drivers of this by first correlating TROPOMI HCHO columns with the Greenhouse Gases Observing Satellite-2 (GOSAT-2) methane columns (Yokota et al., 2009) (Figure S6 in Supporting Information S1). Over those regions with significant T-dependency, the correlation is either insignificant or negative, indicating other drivers rather than methane oxidation. Such T-dependencies may be traced to seasonal changes of wind direction influencing the terrestrial outflow of long-lived VOCs (Gopikrishnan & Kuttippurath, 2021; Wittrock et al., 2006) and localized VOCs emitted by phytoplankton activities (Conte et al., 2020; Halsey et al., 2023), admitting high uncertainties in oceanic emissions (Arnold et al., 2009; Booge et al., 2016, 2018; Myriokefalitakis et al., 2010).

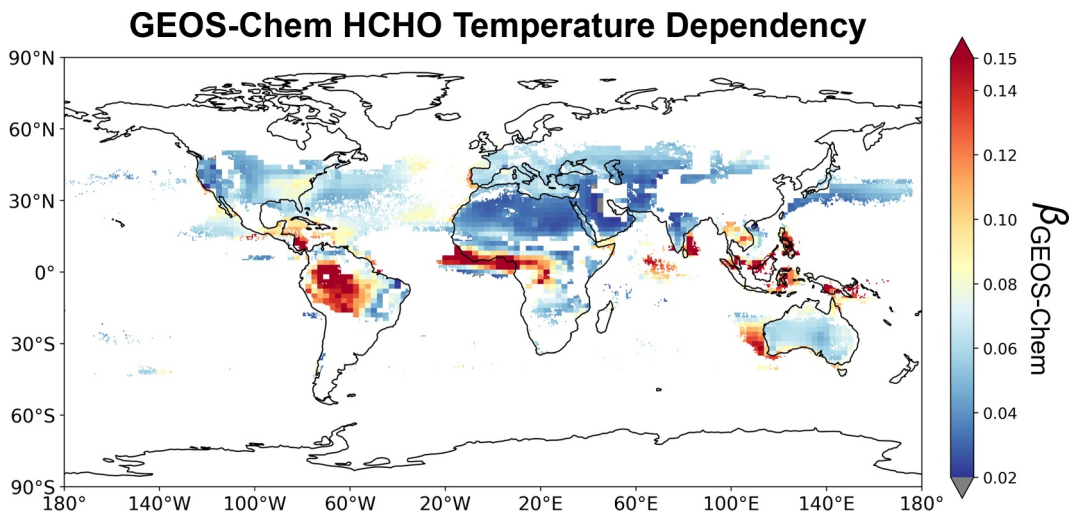

Figure 3. Global temperature (T-) dependency of GEOS-Chem HCHO columns. $\beta_{\text{GEOS-Chem}}$ (unit: ln (10^{15} molecules cm^{-2}) K^{-1}) is defined as $\Omega_{\text{GEOS-Chem}} = \exp(\alpha_{\text{GEOS-Chem}} + \beta_{\text{GEOS-Chem}}\, T + \varepsilon)$ (Text S2 in Supporting Information S1). $\Omega_{\text{GEOS-Chem}}$ is the monthly GEOS-Chem HCHO column, corrected with the TROPOMI averaging kernels. $\alpha_{\text{GEOS-Chem}}$ is the baseline, and T denotes the 2-m temperature (>285 K). Only showing are biogenic-dominated grids with significant $\beta_{\text{GEOS-Chem}}$ (p-value <0.05) and high dependency ($R^2 > 0.5$). Low T-dependency regions (<0.02; gray) are excluded from further analysis, consistent with β_{TROPOMI} in Figure 2.

4. Interpreting β_{TROPOMI} With MEGAN Implemented in GEOS-Chem

To interpret how β_{TROPOMI} varies spatially and across PFTs, we use the GEOS-Chem model (Text S1 in Supporting Information S1) that links HCHO columns with BVOC emissions driven by an array of environmental factors through the MEGAN module. GEOS-Chem HCHO vertical profiles are sampled locally at TROPOMI over-passing time (13:00–14:00) and then corrected with TROPOMI averaging kernels (Text S2 in Supporting Information S1). As shown in Figure S7 of Supporting Information S1, GEOS-Chem HCHO columns, in general, are linearly related to TROPOMI HCHO columns, supporting the interpretation of TROPOMI HCHO columns with GEOS-Chem, acknowledging that an overall overestimation and underestimation exist (Figure S7 in Supporting Information S1, panel c and d, respectively), which is not reflected by the T-dependency analysis.

We see from Figure 3 that the T-dependency of GEOS-Chem HCHO columns ($\beta_{\text{GEOS-Chem}}$) consistently shows latitudinal variations and hot spots as reflected by β_{TROPOMI} (Figure 1), but with an overestimation than TROPOMI. Such overestimation is reflected in the overestimation of HCHO column variations (Figure S7 in Supporting Information S1, panel b). GEOS-Chem also overestimates the T-dependency in the Indian Ocean, off the coast of Western Australia, and around the Caribbean up to two times. This leads to the hypothesis that the ocean sources of HCHO may undermine the HCHO T-dependency offshore brought by seasonal winds (Gopikrishnan & Kuttippurath, 2021) since GEOS-Chem includes no ocean contribution. Additionally, $\beta_{\text{GEOS-Chem}}$ coincides highly ($r = 0.87$) with β_{TROPOMI} on the PFT level (Figure 2). On average, $\beta_{\text{GEOS-Chem}}$ is 16.0% higher than β_{TROPOMI}, with discrepancy ranging from 6.1% (PFT 14, Warm C4 Grass) to 62.8% (PFT 8, Broadleaf Deciduous Boreal Tree).

To evaluate how BVOC emissions contribute to such discrepancy between $\beta_{\text{GEOS-Chem}}$ and β_{TROPOMI}, we refer to the calculation of the temperature activity factor (γ_T) in the MEGAN module implemented in the GEOS-Chem model and perturb it using information from TROPOMI as follows:

$$\gamma_T' = \gamma_T \times \sum_{i=1}^{15} \chi_i \exp\left(\Delta\beta_i (T - T_s)\right) \tag{2}$$

where χ_i is the fractional area from PFT i coverage within the grid, $\Delta\beta_i = \beta_{\text{TROPOMI},\,i} - \beta_{\text{GEOS-Chem},\,i}$ corrects the discrepancy between β_{TROPOMI} and $\beta_{\text{GEOS-Chem}}$ for PFT i (Table S2 in Supporting Information S1), T and T_s is the respective air temperature and standard temperature as described in the MEGAN model (Chen et al., 2023;

Guenther et al., 1993; Zeng et al., 2023) and set to be 303 K in GEOS-Chem. T-dependencies of HCHO columns from the perturbed GEOS-Chem simulation as denoted as $\beta'_{\text{GEOS-Chem}}$.

We see from Figure 2 that $\beta'_{\text{GEOS-Chem}}$ shows varying degrees of improvement compared with the default $\beta_{\text{GEOS-Chem}}$, with PFT 4 (Broadleaf Evergreen Tropical Tree) and PFT 14 (Warm C4 Grass) being the most efficient (72.9% and 90.8%, respectively). This indicates that BVOC emissions T-dependencies contribute mainly to HCHO columns T-dependencies at the lower and middle latitudes, where BVOC emissions are abundant. Our simulation shows that isoprene emission flux from PFT 4 under high temperatures, such as 315 K, is overestimated by at least 11% ($\sim 1.2 \times 10^{-9}$ kg m^{-2} s^{-1}) by the default GEOS-Chem. The result is consistent with the reported mismatch between MEGAN estimation and satellite-derived isoprene emissions (Barkley et al., 2012, 2013), recognizing that the degree of overestimation may vary depending on the versions of MEGAN and the landcover therein, and the meteorological information used in GEOS-Chem.

The remaining discrepancy between $\beta_{\text{GEOS-Chem}}$ and β_{TROPOMI} for other PFTs is likely due to the insensitivity of GEOS-Chem HCHO columns to BVOC emissions. To verify this, we replace the default isoprene emissions with the measured fluxes (Seco et al., 2022) in a boreal region (PFT 11, Broadleaf Deciduous Boreal Shrub). The sensitivity simulation shows that ~80% of the isoprene emission variation only leads to ~6.0% of the HCHO columns variation (Figure S8 in Supporting Information S1), indicating a weak response of HCHO columns to BVOC emissions. This reminds us that challenges exist when applying satellite HCHO columns as the proxy of BVOC emissions in regions with those PFTs, acknowledging other factors, such as Leaf Area Index (LAI), Aerosol Optical Depth (AOD), nitrogen oxides (NO_x) level, and season transition, also complicate the relationship between HCHO columns and BVOC emissions (Alves et al., 2018; Barkley et al., 2012, 2013; Marais et al., 2012; Strada et al., 2023).

The perturbation improves T-dependency in general but has both reductions and amplifications in the discrepancy of HCHO columns simulation. The discrepancy of HCHO columns mean value reduces in regions where GEOS-Chem has an overall overestimation compared with TROPOMI (mainly Southeast US and tropical regions), while amplifying in underestimation regions (mainly India and Australia) (Figure S9 in Supporting Information S1). On the PFT level, the perturbation improves the total HCHO columns by 1.8% for the Broadleaf Evergreen Tropical Tree, while exacerbating the discrepancy in the rest of the PFTs (0.47%–4.5%).

5. Conclusions

We have used TROPOMI satellite observations to investigate the temperature (T-) dependency of HCHO columns over the globe. The T-dependence of HCHO columns exhibits notable variations across Plant Functional Types (PFTs), with the highest dependency observed in the Broadleaf Evergreen Tropical Tree category. The GEOS-Chem model primarily interprets the T-dependency of HCHO columns at the PFT level, although there is a 16% discrepancy on average. We perturbed the temperature activity factor in MEGAN by introducing TROPOMI HCHO T-dependency information. The main drivers of such a discrepancy are the T-dependency of BVOC emissions for Broadleaf Evergreen Tropical Tree and Warm C4 Grass, and the insensitivity of HCHO columns to BVOC emissions for other PFTs.

We recommend a PFT-specific correction for temperature activity factor over tropical regions in the MEGAN model implemented in the GEOS-Chem, since BVOC T-dependency there interprets most of the HCHO T-dependency, and, although minor, has an improvement on HCHO columns simulation. The updates provide a correction accorded with satellite observation and improve the estimation of BVOC emission and HCHO columns, especially at high temperatures. We find that GEOS-Chem has an 11% ($\sim 1.2 \times 10^{-9}$ kg m^{-2} s^{-1}) of the isoprene emission overestimation compared with satellite observation for Broadleaf Evergreen Tropical Tree area at 315 K. The correction needs further investigation, such as additional model runs, including source attribution of HCHO T-dependency, since the improvement in this study is limited for those PFTs other than tropical regions.

Data Availability Statement

We gratefully acknowledge TROPOMI HCHO product (Copernicus Sentinel-5P, 2020), MERRA-2 T2M product (Global Modeling and Assimilation Office, 2015) implemented in GEOS-Chem with the description access at http://wiki.seas.harvard.edu/geos-chem/index.php/MERRA-2_implementation_details, GOSAT methane

product (Japan Aerospace Exploration Agency, 2018). Oversampling code, data analysis scripts, and GEOS-Chem configuration files are available at the Zenodo repository (Li et al., 2024).

Acknowledgments
This work is funded by the National Natural Science Foundation of China (42375090), National Key Research and Development Program of China (2023YFC3706205), Shenzhen Key Laboratory of Precision Measurement and Early Warning Technology for Urban Environmental Health Risks (ZDSYS20220606100604008), Guangdong Basic and Applied Basic Research Foundation (2021A1515110713), Guangdong University Research Project Science Team (2021KCXTD004), Major Talent Project of Guangdong Province (2021QN020924), Shenzhen Science and Technology Program (KQTD20210811090048025, JCYJ20220530115404009), and High level of special funds (G030290001). This work is supported by the Center for Computational Science and Engineering at Southern University of Science and Technology.

References

Abbot, D. S., Palmer, P. I., Martin, R. V., Chance, K. V., Jacob, D. J., & Guenther, A. (2003). Seasonal and interannual variability of North American isoprene emissions as determined by formaldehyde column measurements from space. *Geophysical Research Letters*, *30*(17). https://doi.org/10.1029/2003GL017336

Alves, E. G., Santana, R. A., Dias-Júnior, C. Q., Botía, S., Taylor, T., Yáñez-Serrano, A. M., et al. (2023). Intra- and interannual changes in isoprene emission from central Amazonia. *Atmospheric Chemistry and Physics*, *23*(14), 8149–8168. https://doi.org/10.5194/acp-23-8149-2023

Alves, E. G., Tóta, J., Turnipseed, A., Guenther, A. B., Vega Bustillos, J. O. W., Santana, R. A., et al. (2018). Leaf phenology as one important driver of seasonal changes in isoprene emissions in central Amazonia. *Biogeosciences*, *15*(13), 4019–4032. https://doi.org/10.5194/bg-15-4019-2018

Arneth, A., Monson, R. K., Schurgers, G., Niinemets, Ü., & Palmer, P. I. (2008). Why are estimates of global terrestrial isoprene emissions so similar (and why is this not so for monoterpenes)? *Atmospheric Chemistry and Physics*, *8*(16), 4605–4620. https://doi.org/10.5194/acp-8-4605-2008

Arneth, A., Schurgers, G., Lathiere, J., Duhl, T., Beerling, D. J., Hewitt, C. N., et al. (2011). Global terrestrial isoprene emission models: Sensitivity to variability in climate and vegetation. *Atmospheric Chemistry and Physics*, *11*(15), 8037–8052. https://doi.org/10.5194/acp-11-8037-2011

Arnold, S. R., Spracklen, D. V., Williams, J., Yassaa, N., Sciare, J., Bonsang, B., et al. (2009). Evaluation of the global oceanic isoprene source and its impacts on marine organic carbon aerosol. *Atmospheric Chemistry and Physics*, *9*(4), 1253–1262. https://doi.org/10.5194/acp-9-1253-2009

Barkley, M. P., Kurosu, T. P., Chance, K., De Smedt, I., Van Roozendael, M., Arneth, A., et al. (2012). Assessing sources of uncertainty in formaldehyde air mass factors over tropical South America: Implications for top-down isoprene emission estimates. *Journal of Geophysical Research*, *117*(D13). https://doi.org/10.1029/2011JD016827

Barkley, M. P., Smedt, I. D., Van Roozendael, M., Kurosu, T. P., Chance, K., Arneth, A., et al. (2013). Top-down isoprene emissions over tropical South America inferred from SCIAMACHY and OMI formaldehyde columns. *Journal of Geophysical Research: Atmospheres*, *118*(12), 6849–6868. https://doi.org/10.1002/jgrd.50552

Bey, I., Jacob, D. J., Yantosca, R. M., Logan, J. A., Field, B. D., Fiore, A. M., et al. (2001). Global modeling of tropospheric chemistry with assimilated meteorology: Model description and evaluation. *Journal of Geophysical Research*, *106*(D19), 23073–23095. https://doi.org/10.1029/2001JD000807

Blonder, B., & Michaletz, S. T. (2018). A model for leaf temperature decoupling from air temperature. *Agricultural and Forest Meteorology*, *262*, 354–360. https://doi.org/10.1016/j.agrformet.2018.07.012

Bonan, G. B., Levis, S., Kergoat, L., & Oleson, K. W. (2002). Landscapes as patches of plant functional types: An integrating concept for climate and ecosystem models. *Global Biogeochemical Cycles*, *16*(2), 5-1–5-23. https://doi.org/10.1029/2000GB001360

Booge, D., Marandino, C. A., Schlundt, C., Palmer, P. I., Schlundt, M., Atlas, E. L., et al. (2016). Can simple models predict large-scale surface ocean isoprene concentrations? *Atmospheric Chemistry and Physics*, *16*(18), 11807–11821. https://doi.org/10.5194/acp-16-11807-2016

Booge, D., Schlundt, C., Bracher, A., Endres, S., Zäncker, B., & Marandino, C. A. (2018). Marine isoprene production and consumption in the mixed layer of the surface ocean—A field study over two oceanic regions. *Biogeosciences*, *15*(2), 649–667. https://doi.org/10.5194/bg-15-649-2018

Bourtsoukidis, E., Pozzer, A., Williams, J., Makowski, D., Peñuelas, J., Matthaios, V. N., et al. (2024). High temperature sensitivity of monoterpene emissions from global vegetation. *Communications Earth & Environment*, *5*(1), 23. https://doi.org/10.1038/s43247-023-01175-9

Cao, Y., Yue, X., Lei, Y., Zhou, H., Liao, H., Song, Y., et al. (2021). Identifying the drivers of modeling uncertainties in isoprene emissions: Schemes versus meteorological forcings. *Journal of Geophysical Research: Atmospheres*, *126*(18). https://doi.org/10.1029/2020JD034242

Chan, K. L., Wiegner, M., van Geffen, J., De Smedt, I., Alberti, C., Cheng, Z., et al. (2020). MAX-DOAS measurements of tropospheric NO_2 and HCHO in Munich and the comparison to OMI and TROPOMI satellite observations. *Atmospheric Measurement Techniques*, *13*(8), 4499–4520. https://doi.org/10.5194/amt-13-4499-2020

Chance, K., Palmer, P. I., Spurr, R. J. D., Martin, R. V., Kurosu, T. P., & Jacob, D. J. (2000). Satellite observations of formaldehyde over North America from GOME. *Geophysical Research Letters*, *27*(21), 3461–3464. https://doi.org/10.1029/2000GL011857

Chen, X., Gong, D., Lin, Y., Xu, Q., Wang, Y., Liu, S., et al. (2023). Emission characteristics of biogenic volatile organic compounds in a subtropical pristine forest of southern China. *Journal of Environmental Sciences*, *148*, 665–682. https://doi.org/10.1016/j.jes.2023.09.041

Conte, L., Szopa, S., Aumont, O., Gros, V., & Bopp, L. (2020). Sources and sinks of isoprene in the global open ocean: Simulated patterns and emissions to the atmosphere. *Journal of Geophysical Research: Oceans*, *125*(9), e2019JC015946. https://doi.org/10.1029/2019JC015946

Copernicus Sentinel-5P (processed by ESA). (2020). TROPOMI level 2 formaldehyde total column products Version 02 [Dataset]. European Space Agency. https://doi.org/10.5270/S5P-vg1i7t0

Curci, G., Palmer, P. I., Kurosu, T. P., Chance, K., & Visconti, G. (2010). Estimating European volatile organic compound emissions using satellite observations of formaldehyde from the Ozone Monitoring Instrument. *Atmospheric Chemistry and Physics*, *10*(23), 11501–11517. https://doi.org/10.5194/acp-10-11501-2010

De Smedt, I., Müller, J. F., Stavrakou, T., van der A, R., Eskes, H., & Van Roozendael, M. (2008). Twelve years of global observations of formaldehyde in the troposphere using GOME and SCIAMACHY sensors. *Atmospheric Chemistry and Physics*, *8*(16), 4947–4963. https://doi.org/10.5194/acp-8-4947-2008

De Smedt, I., Pinardi, G., Vigouroux, C., Compernolle, S., Bais, A., Benavent, N., et al. (2021). Comparative assessment of TROPOMI and OMI formaldehyde observations and validation against MAX-DOAS network column measurements. *Atmospheric Chemistry and Physics*, *21*(16), 12561–12593. https://doi.org/10.5194/acp-21-12561-2021

De Smedt, I., Stavrakou, T., Hendrick, F., Danckaert, T., Vlemmix, T., Pinardi, G., et al. (2015). Diurnal, seasonal and long-term variations of global formaldehyde columns inferred from combined OMI and GOME-2 observations. *Atmospheric Chemistry and Physics*, *15*(21), 12519–12545. https://doi.org/10.5194/acp-15-12519-2015

De Smedt, I., Theys, N., Yu, H., Danckaert, T., Lerot, C., Compernolle, S., et al. (2018). Algorithm theoretical baseline for formaldehyde retrievals from S5P TROPOMI and from the QA4ECV project. *Atmospheric Measurement Techniques*, *11*(4), 2395–2426. https://doi.org/10.5194/amt-11-2395-2018

De Smedt, I., Van Roozendael, M., Stavrakou, T., Müller, J. F., Lerot, C., Theys, N., et al. (2012). Improved retrieval of global tropospheric formaldehyde columns from GOME-2/MetOp-A addressing noise reduction and instrumental degradation issues. *Atmospheric Measurement Techniques*, *5*(11), 2933–2949. https://doi.org/10.5194/amt-5-2933-2012

Duncan, B. N., Yoshida, Y., Damon, M. R., Douglass, A. R., & Witte, J. C. (2009). Temperature dependence of factors controlling isoprene emissions. *Geophysical Research Letters*, *36*(5). https://doi.org/10.1029/2008GL037090

Fauset, S., Freitas, H. C., Galbraith, D. R., Sullivan, M. J., Aidar, M. P., Joly, C. A., et al. (2018). Differences in leaf thermoregulation and water use strategies between three co-occurring Atlantic forest tree species. *Plant, Cell and Environment*, *41*(7), 1618–1631. https://doi.org/10.1111/pce.13208

Garcia, S., Jardine, K., Souza, V. F. D., de Souza, R. A., Duvoisin Junior, S., & Gonçalves, J. F. D. C. (2019). Reassimilation of leaf internal CO_2 contributes to isoprene emission in the Neotropical Species Inga edulis Mart. *Forests*, *10*(6), 472. https://doi.org/10.3390/f10060472

Global Modeling and Assimilation Office (GMAO). (2015). MERRA-2 tavg3_3d_tdt_Np: 3d,3-Hourly, time-averaged, pressure-level, assimilation, temperature tendencies V5.12.4 [Dataset]. Goddard Earth Sciences Data and Information Services Center (GES DISC). https://doi.org/10.5067/9NCR9DDDOPFI

Goldberg, D. L., Harkey, M., de Foy, B., Judd, L., Johnson, J., Yarwood, G., & Holloway, T. (2022). Evaluating NO_x emissions and their effect on O_3 production in Texas using TROPOMI NO_2 and HCHO. *Atmospheric Chemistry and Physics*, *22*(16), 10875–10900. https://doi.org/10.5194/acp-22-10875-2022

Goldstein, A. H., Goulden, M. L., Munger, J. W., Wofsy, S. C., & Geron, C. D. (1998). Seasonal course of isoprene emissions from a midlatitude deciduous forest. *Journal of Geophysical Research*, *103*(D23), 31045–31056. https://doi.org/10.1029/98JD02708

Gopikrishnan, G. S., & Kuttippurath, J. (2021). A decade of satellite observations reveal significant increase in atmospheric formaldehyde from shipping in Indian Ocean. *Atmospheric Environment*, *246*, 118095. https://doi.org/10.1016/j.atmosenv.2020.118095

Guenther, A., Hewitt, C. N., Erickson, D., Fall, R., Geron, C., Graedel, T., et al. (1995). A global model of natural volatile organic compound emissions. *Journal of Geophysical Research*, *100*(D5), 8873–8892. https://doi.org/10.1029/94JD02950

Guenther, A., Jiang, X., Heald, C., Sakulyanontvittaya, T., Duhl, T., Emmons, L., & Wang, X. (2012). The model of emissions of gases and aerosols from nature version 2.1 (MEGAN2.1): An extended and updated framework for modeling biogenic emissions. *Geoscientific Model Development*, *5*(6), 1471–1492. https://doi.org/10.5194/gmd-5-1471-2012

Guenther, A., Karl, T., Harley, P., Wiedinmyer, C., Palmer, P. I., & Geron, C. (2006). Estimates of global terrestrial isoprene emissions using MEGAN (model of emissions of gases and aerosols from nature). *Atmospheric Chemistry and Physics*, *6*(11), 3181–3210. https://doi.org/10.5194/acp-6-3181-2006

Guenther, A. B., Zimmerman, P. R., Harley, P. C., Monson, R. K., & Fall, R. (1993). Isoprene and monoterpene emission rate variability: Model evaluations and sensitivity analyses. *Journal of Geophysical Research*, *98*(D7), 12609–12617. https://doi.org/10.1029/93JD00527

Halsey, K. H., & Giovannoni, S. J. (2023). Biological controls on marine volatile organic compound emissions: A balancing act at the sea-air interface. *Earth-Science Reviews*, *240*, 104360. https://doi.org/10.1016/j.earscirev.2023.104360

Harley, P., Otter, L., Guenther, A., & Greenberg, J. (2003). Micrometeorological and leaf-level measurements of isoprene emissions from a southern African savanna. *Journal of Geophysical Research*, *108*(D13). https://doi.org/10.1029/2002JD002592

Harley, P., Vasconcellos, P., Vierling, L., Pinheiro, C. C. D. S., Greenberg, J., Guenther, A., et al. (2004). Variation in potential for isoprene emissions among Neotropical forest sites. *Global Change Biology*, *10*(5), 630–650. https://doi.org/10.1111/j.1529-8817.2003.00760.x

Heald, C. L., Wilkinson, M. J., Monson, R. K., Alo, C. A., Wang, G., & Guenther, A. (2009). Response of isoprene emission to ambient CO_2 changes and implications for global budgets. *Global Change Biology*, *15*(5), 1127–1140. https://doi.org/10.1111/j.1365-2486.2008.01802.x

Hofzumahaus, A., Rohrer, F., Lu, K., Bohn, B., Brauers, T., Chang, C.-C., et al. (2009). Amplified trace gas removal in the troposphere. *Science*, *324*(5935), 1702–1704. https://doi.org/10.1126/science.1164566

Jaars, K., van Zyl, P. G., Beukes, J. P., Hellén, H., Vakkari, V., Josipovic, M., et al. (2016). Measurements of biogenic volatile organic compounds at a grazed savannah grassland agricultural landscape in South Africa. *Atmospheric Chemistry and Physics*, *16*(24), 15665–15688. https://doi.org/10.5194/acp-16-15665-2016

Janssen, R. H. H., Vilà-Guerau de Arellano, J., Jimenez, J. L., Ganzeveld, L. N., Robinson, N. H., Allan, J. D., et al. (2013). Influence of boundary layer dynamics and isoprene chemistry on the organic aerosol budget in a tropical forest. *Journal of Geophysical Research: Atmospheres*, *118*(16), 9351–9366. https://doi.org/10.1002/jgrd.50672

Japan Aerospace Exploration Agency (JAXA). (2018). GOSAT-2 (Greenhouse gases observing satellite-2)/Ibuki-2 [Dataset]. https://earth.esa.int/eogateway/catalog/gosat-tanso-fts-and-cai-full-archive-and-new-products?category=Data

Jardine, K., Chambers, J., Alves, E. G., Teixeira, A., Garcia, S., Holm, J., et al. (2014). Dynamic balancing of isoprene carbon sources reflects photosynthetic and photorespiratory responses to temperature stress. *Plant Physiology*, *166*(4), 2051–2064. https://doi.org/10.1104/pp.114.247494

Jardine, K. J., Jardine, A. B., Souza, V. F., Carneiro, V., Ceron, J. V., Gimenez, B. O., et al. (2016). Methanol and isoprene emissions from the fast growing tropical pioneer species Vismia guianensis (Aubl.) Pers. (Hypericaceae) in the central Amazon forest. *Atmospheric Chemistry and Physics*, *16*(10), 6441–6452. https://doi.org/10.5194/acp-16-6441-2016

Jin, X., Fiore, A. M., & Cohen, R. C. (2023). Space-based observations of ozone precursors within California Wildfire Plumes and the impacts on ozone-NO_x-VOC chemistry. *Environmental Science and Technology*, *57*(39), 14648–14660. https://doi.org/10.1021/acs.est.3c04411

Kaiser, J., Jacob, D. J., Zhu, L., Travis, K. R., Fisher, J. A., González Abad, G., et al. (2018). High-resolution inversion of OMI formaldehyde columns to quantify isoprene emission on ecosystem-relevant scales: Application to the southeastsoutheast US. *Atmospheric Chemistry and Physics*, *18*(8), 5483–5497. https://doi.org/10.5194/acp-18-5483-2018

Kroll, J. H., Ng, N. L., Murphy, S. M., Flagan, R. C., & Seinfeld, J. H. (2006). Secondary organic aerosol formation from isoprene photooxidation. *Environmental Science and Technology*, *40*(6), 1869–1877. https://doi.org/10.1021/es0524301

Langford, B., Cash, J., Acton, W. J. F., Valach, A. C., Hewitt, C. N., Fares, S., et al. (2017). Isoprene emission potentials from European oak forests derived from canopy flux measurements: An assessment of uncertainties and inter-algorithm variability. *Biogeosciences*, *14*(23), 5571–5594. https://doi.org/10.5194/bg-14-5571-2017

Langford, B., House, E., Valach, A., Hewitt, C. N., Artaxo, P., Barkley, M. P., et al. (2022). Seasonality of isoprene emissions and oxidation products above the remote Amazon. *Environmental Sciences: Atmosphere*, *2*, 230–240. https://doi.org/10.1039/D1EA00057H

Lehning, A., Zimmer, I., Steinbrecher, R., Brüggemann, N., & Schnitzler, J. P. (1999). Isoprene synthase activity and its relation to isoprene emission in Quercus Robur L-leaves. *Plant, Cell and Environment*, *22*(5), 495–504. https://doi.org/10.1046/j.1365-3040.1999.00425.x

Li, K., Jacob, D. J., Liao, H., Qiu, Y., Shen, L., Zhai, S., et al. (2021). Ozone pollution in the North China Plain spreading into the late-winter haze season. *Proceedings of the National Academy of Sciences*, *118*(10), e2015797118. https://doi.org/10.1073/pnas.2015797118

Li, X., Zhu, L., De Smedt, I., Sun, W., Chen, Y., Shu, L., et al. (2024). Open Research for Global temperature dependency of biogenic HCHO columns observed from space: Interpretation of TROPOMI results using GEOS-Chem model [Software]. *Zenodo*. https://doi.org/10.5281/zenodo.13955391

Litvak, M. E., Loreto, F., Harley, P. C., Sharkey, T. D., & Monson, R. K. (1996). The response of isoprene emission rate and photosynthetic rate to photon flux and nitrogen supply in aspen and white oak trees. *Plant, Cell and Environment*, *19*(5), 549–559. https://doi.org/10.1111/j.1365-3040.1996.tb00388.x

Marais, E. A., Jacob, D. J., Kurosu, T. P., Chance, K., Murphy, J. G., Reeves, C., et al. (2012). Isoprene emissions in Africa inferred from OMI observations of formaldehyde columns. *Atmospheric Chemistry and Physics*, *12*(14), 6219–6235. https://doi.org/10.5194/acp-12-6219-2012

McKinney, K., Lee, B., Vasta, A., Pho, T., & Munger, J. (2011). Emissions of isoprenoids and oxygenated biogenic volatile organic compounds from a New England mixed forest. *Atmospheric Chemistry and Physics*, *11*(10), 4807–4831. https://doi.org/10.5194/acp-11-4807-2011

Millet, D. B., Jacob, D. J., Boersma, K. F., Fu, T.-M., Kurosu, T. P., Chance, K., et al. (2008). Spatial distribution of isoprene emissions from North America derived from formaldehyde column measurements by the OMI satellite sensor. *Journal of Geophysical Research*, *113*(D2). https://doi.org/10.1029/2007JD008950

Millet, D. B., Jacob, D. J., Turquety, S., Hudman, R. C., Wu, S., Fried, A., et al. (2006). Formaldehyde distribution over North America: Implications for satellite retrievals of formaldehyde columns and isoprene emission. *Journal of Geophysical Research*, *111*(D24). https://doi.org/10.1029/2005JD006853

Misztal, P. K., Avise, J. C., Karl, T., Scott, K., Jonsson, H. H., Guenther, A. B., & Goldstein, A. H. (2016). Evaluation of regional isoprene emission factors and modeled fluxes in California. *Atmospheric Chemistry and Physics*, *16*(15), 9611–9628. https://doi.org/10.5194/acp-16-9611-2016

Misztal, P. K., Nemitz, E., Langford, B., Di Marco, C., Phillips, G., Hewitt, C., et al. (2011). Direct ecosystem fluxes of volatile organic compounds from oil palms in South-East Asia. *Atmospheric Chemistry and Physics*, *11*(17), 8995–9017. https://doi.org/10.5194/acp-11-8995-2011

Monson, R. K., Jaeger, C. H., Adams, W. W., III, Driggers, E. M., Silver, G. M., & Fall, R. (1992). Relationships among isoprene emission rate, photosynthesis, and isoprene synthase activity as influenced by temperature. *Plant Physiology*, *98*(3), 1175–1180. https://doi.org/10.1104/pp.98.3.1175

Myriokefalitakis, S., Vignati, E., Tsigaridis, K., Papadimas, C., Sciare, J., Mihalopoulos, N., et al. (2010). Global modeling of the oceanic source of organic aerosols. *Advances in Meteorology*, *2010*(1), 939171. https://doi.org/10.1155/2010/939171

Naimark, J. G., Fiore, A. M., Jin, X., Wang, Y., Klovenski, E., & Braneon, C. (2021). Evaluating drought responses of surface ozone precursor proxies: Variations with land cover type, precipitation, and temperature. *Geophysical Research Letters*, *48*(7), e2020GL091520. https://doi.org/10.1029/2020GL091520

Pacifico, F., Folberth, G. A., Jones, C. D., Harrison, S. P., & Collins, W. J. (2012). Sensitivity of biogenic isoprene emissions to past, present, and future environmental conditions and implications for atmospheric chemistry. *Journal of Geophysical Research*, *117*(D22). https://doi.org/10.1029/2012JD018276

Palmer, P. I., Abbot, D. S., Fu, T.-M., Jacob, D. J., Chance, K., Kurosu, T. P., et al. (2006). Quantifying the seasonal and interannual variability of North American isoprene emissions using satellite observations of the formaldehyde column. *Journal of Geophysical Research*, *111*(D12). https://doi.org/10.1029/2005JD006689

Palmer, P. I., Jacob, D. J., Fiore, A. M., Martin, R. V., Chance, K., & Kurosu, T. P. (2003). Mapping isoprene emissions over North America using formaldehyde column observations from space. *Journal of Geophysical Research*, *108*(D6). https://doi.org/10.1029/2002JD002153

Palmer, P. I., & Shaw, S. L. (2005). Quantifying global marine isoprene fluxes using MODIS chlorophyll observations. *Geophysical Research Letters*, *32*(9), L09805. https://doi.org/10.1029/2005GL022592

Pétron, G., Harley, P., Greenberg, J., & Guenther, A. (2001). Seasonal temperature variations influence isoprene emission. *Geophysical Research Letters*, *28*(9), 1707–1710. https://doi.org/10.1029/2000GL011583

Pressley, S., Lamb, B., Westberg, H., Flaherty, J., Chen, J., & Vogel, C. (2005). Long-term isoprene flux measurements above a northern hardwood forest. *Journal of Geophysical Research*, *110*(D7). https://doi.org/10.1029/2004JD005523

Pu, D., Zhu, L., De Smedt, I., Li, X., Sun, W., Wang, D., et al. (2022). Response of anthropogenic volatile organic compound emissions to urbanization in Asia probed with TROPOMI and VIIRS satellite observations. *Geophysical Research Letters*, *49*(18), e2022GL099470. https://doi.org/10.1029/2022GL099470

Rasulov, B., Hüve, K., Bichele, I., Laisk, A., & Niinemets, Ü. (2010). Temperature response of isoprene emission in vivo reflects a combined effect of substrate limitations and isoprene synthase activity: A kinetic analysis. *Plant Physiology*, *154*(3), 1558–1570. https://doi.org/10.1104/pp.110.162081

Rhew, R. C., Deventer, M. J., Turnipseed, A. A., Warneke, C., Ortega, J., Shen, S., et al. (2017). Ethene, propene, butane and isoprene emissions from a ponderosa pine forest measured by relaxed eddy accumulation. *Atmospheric Chemistry and Physics*, *17*(21), 13417–13438. https://doi.org/10.5194/acp-17-13417-2017

Ryan, R. G., Marais, E. A., Gershenson-Smith, E., Ramsay, R., Muller, J. P., Tirpitz, J. L., & Frieß, U. (2023). Measurement report: MAX-DOAS measurements characterise central London ozone pollution episodes during 2022 heatwaves. *Atmospheric Chemistry and Physics*, *23*(12), 7121–7139. https://doi.org/10.5194/acp-23-7121-2023

Ryan, R. G., Rhodes, S., Tully, M., & Schofield, R. (2020a). Surface ozone exceedances in Melbourne, Australia are shown to be under NO_x control, as demonstrated using formaldehyde: NO_2 and glyoxal: Formaldehyde ratios. *Science of the Total Environment*, *749*, 141460. https://doi.org/10.1016/j.scitotenv.2020.141460

Ryan, R. G., Silver, J. D., Querel, R., Smale, D., Rhodes, S., Tully, M., et al. (2020b). Comparison of formaldehyde tropospheric columns in Australia and New Zealand using MAX-DOAS, FTIR and TROPOMI. *Atmospheric Measurement Techniques*, *13*(12), 6501–6519. https://doi.org/10.5194/amt-13-6501-2020

Seco, R., Holst, T., Davie-Martin, C. L., Simin, T., Guenther, A., Pirk, N., et al. (2022). Strong isoprene emission response to temperature in tundra vegetation. *Proceedings of the National Academy of Sciences*, *119*(38), e2118014119. https://doi.org/10.1073/pnas.2118014119

Sharkey, T. D., Wiberley, A. E., & Donohue, A. R. (2007). Isoprene emission from plants: Why and how. *Annals of Botany*, *101*(1), 5–18. https://doi.org/10.1093/aob/mcm240

Shim, C., Wang, Y., Choi, Y., Palmer, P. I., Abbot, D. S., & Chance, K. (2005). Constraining global isoprene emissions with Global Ozone Monitoring Experiment (GOME) formaldehyde column measurements. *Journal of Geophysical Research*, *110*(D24). https://doi.org/10.1029/2004JD005629

Sindelarova, K., Granier, C., Bouarar, I., Guenther, A., Tilmes, S., Stavrakou, T., et al. (2014). Global data set of biogenic VOC emissions calculated by the MEGAN model over the last 30 years. *Atmospheric Chemistry and Physics*, *14*(17), 9317–9341. https://doi.org/10.5194/acp-14-9317-2014

Steiner, A. L., Davis, A. J., Sillman, S., Owen, R. C., Michalak, A. M., & Fiore, A. M. (2010). Observed suppression of ozone formation at extremely high temperatures due to chemical and biophysical feedbacks. *Proceedings of the National Academy of Sciences*, *107*(46), 19685–19690. https://doi.org/10.1073/pnas.1008336107

Still, C. J., Page, G., Rastogi, B., Griffith, D. M., Aubrecht, D. M., Kim, Y., et al. (2022). No evidence of canopy-scale leaf thermoregulation to cool leaves below air temperature across a range of forest ecosystems. *Proceedings of the National Academy of Sciences*, *119*(38), e2205682119. https://doi.org/10.1073/pnas.2205682119

Stoy, P. C., Trowbridge, A. M., Siqueira, M. B., Freire, L. S., Phillips, R. P., Jacobs, L., et al. (2021). Vapor pressure deficit helps explain biogenic volatile organic compound fluxes from the forest floor and canopy of a temperate deciduous forest. *Oecologia*, *197*(4), 971–988. https://doi.org/10.1007/s00442-021-04891-1

Strada, S., Fernández-Martínez, M., Peñuelas, J., Bauwens, M., Stavrakou, T., Verger, A., & Giorgi, F. (2023). Disentangling temperature and water stress contributions to trends in isoprene emissions using satellite observations of formaldehyde, 2005–2016. *Atmospheric Environment*, *295*, 119530. https://doi.org/10.1016/j.atmosenv.2022.119530

Sun, W., Zhu, L., De Smedt, I., Bai, B., Pu, D., Chen, Y., et al. (2021). Global Significant changes in formaldehyde (HCHO) columns observed from space at the early stage of the COVID-19 pandemic. *Geophysical Research Letters*, *48*(4), 2e020GL091265. https://doi.org/10.1029/2020GL091265

Surl, L., Palmer, P. I., & González Abad, G. (2018). Which processes drive observed variations of HCHO columns over India? *Atmospheric Chemistry and Physics*, *18*(7), 4549–4566. https://doi.org/10.5194/acp-18-4549-2018

Tai, A. P. K., Mickley, L. J., Heald, C. L., & Wu, S. (2013). Effect of CO_2 inhibition on biogenic isoprene emission: Implications for air quality under 2000 to 2050 changes in climate, vegetation, and land use. *Geophysical Research Letters*, *40*(13), 3479–3483. https://doi.org/10.1002/grl.50650

Van Meeningen, Y., Schurgers, G., Rinnan, R., & Holst, T. (2017). Isoprenoid emission response to changing light conditions of English oak, European beech and Norway spruce. *Biogeosciences*, *14*(18), 4045–4060. https://doi.org/10.5194/bg-14-4045-2017

Veefkind, J. P., Aben, I., McMullan, K., Förster, H., de Vries, J., Otter, G., et al. (2012). TROPOMI on the ESA Sentinel-5 precursor: A GMES mission for global observations of the atmospheric composition for climate, air quality and ozone layer applications. *Remote Sensing of Environment*, *120*, 70–83. https://doi.org/10.1016/j.rse.2011.09.027

Vigouroux, C., Langerock, B., Bauer Aquino, C. A., Blumenstock, T., Cheng, Z., De Mazière, M., et al. (2020). TROPOMI–Sentinel-5 Precursor formaldehyde validation using an extensive network of ground-based Fourier-transform infrared stations. *Atmospheric Measurement Techniques*, *13*(7), 3751–3767. https://doi.org/10.5194/amt-13-3751-2020

Wang, X., Zhang, Y., Tan, Y., Tan, Y., Bai, J., Gu, D., et al. (2022). Effects of light on the emissions of biogenic isoprene and monoterpenes: A review. *Atmospheric Pollution Research*, *13*(5), 101397. https://doi.org/10.1016/j.apr.2022.101397

Wei, D., Fuentes, J. D., Gerken, T., Chamecki, M., Trowbridge, A. M., Stoy, P. C., et al. (2018). Environmental and biological controls on seasonal patterns of isoprene above a rain forest in central Amazonia. *Agricultural and Forest Meteorology*, *256–257*, 391–406. https://doi.org/10.1016/j.agrformet.2018.03.024

Wittrock, F., Richter, A., Oetjen, H., Burrows, J. P., Kanakidou, M., Myriokefalitakis, S., et al. (2006). Simultaneous global observations of glyoxal and formaldehyde from space. *Geophysical Research Letters*, *33*(16). https://doi.org/10.1029/2006GL026310

Wolfe, G. M., Kaiser, J., Hanisco, T. F., Keutsch, F. N., de Gouw, J. A., Gilman, J. B., et al. (2016). Formaldehyde production from isoprene oxidation across NO_x regimes. *Atmospheric Chemistry and Physics*, *16*(4), 2597–2610. https://doi.org/10.5194/acp-16-2597-2016

Wu, K., Yang, X., Chen, D., Gu, S., Lu, Y., Jiang, Q., et al. (2020). Estimation of biogenic VOC emissions and their corresponding impact on ozone and secondary organic aerosol formation in China. *Atmospheric Research*, *231*, 104656. https://doi.org/10.1016/j.atmosres.2019.104656

Yokota, T., Yoshida, Y., Eguchi, N., Ota, Y., Tanaka, T., Watanabe, H., & Maksyutov, S. (2009). Global concentrations of CO_2 and CH_4 retrieved from GOSAT: First preliminary results. *Sola*, *5*, 160–163. https://doi.org/10.2151/sola.2009–041

Zeng, J., Zhang, Y., Mu, Z., Pang, W., Zhang, H., Wu, Z., et al. (2023). Temperature and light dependency of isoprene and monoterpene emissions from tropical and subtropical trees: Field observations in south China. *Applied Geochemistry*, *155*, 105727. https://doi.org/10.1016/j.apgeochem.2023.105727

Zhang, Y., Li, R., Min, Q., Bo, H., Fu, Y., Wang, Y., & Gao, Z. (2019). The controlling factors of atmospheric formaldehyde (HCHO) in Amazon as seen from satellite. *Earth and Space Science*, *6*(6), 959–971. https://doi.org/10.1029/2019EA000627

Zhao, T., Mao, J., Simpson, W. R., De Smedt, I., Zhu, L., Hanisco, T. F., et al. (2022). Source and variability of formaldehyde (HCHO) at northern high latitudes: An integrated satellite, aircraft, and model study. *Atmospheric Chemistry and Physics*, *22*(11), 7163–7178. https://doi.org/10.5194/acp-22-7163-2022

Zheng, Y., Unger, N., Tadić, J. M., Seco, R., Guenther, A. B., Barkley, M. P., et al. (2017). Drought impacts on photosynthesis, isoprene emission and atmospheric formaldehyde in a mid-latitude forest. *Atmospheric Environment*, *167*, 190–201. https://doi.org/10.1016/j.atmosenv.2017.08.017

Zhu, L., Jacob, D. J., Keutsch, F. N., Mickley, L. J., Scheffe, R., Strum, M., et al. (2017a). Formaldehyde (HCHO) ss a hazardous air pollutant: Mapping surface air concentrations from satellite and inferring cancer risks in the United States. *Environmental Science and Technology*, *51*(10), 5650–5657. https://doi.org/10.1021/acs.est.7b01356

Zhu, L., Jacob, D. J., Mickley, L. J., Marais, E. A., Cohan, D. S., Yoshida, Y., et al. (2014). Anthropogenic emissions of highly reactive volatile organic compounds in eastern Texas inferred from oversampling of satellite (OMI) measurements of HCHO columns. *Environmental Research Letters*, *9*(11), 114004. https://doi.org/10.1088/1748-9326/9/11/114004

Zhu, L., Mickley, L. J., Jacob, D. J., Marais, E. A., Sheng, J., Hu, L., et al. (2017b). Long-term (2005–2014) trends in formaldehyde (HCHO) columns across North America as seen by the OMI satellite instrument: Evidence of changing emissions of volatile organic compounds. *Geophysical Research Letters*, *44*(13), 7079–7086. https://doi.org/10.1002/2017GL073859

Zuo, X., Sun, W., De Smedt, I., Li, X., Liu, S., Pu, D., et al. (2023). Observing downwind structures of Urban HCHO plumes from space: Implications to non-methane volatile organic compound emissions. *Geophysical Research Letters*, *50*(24), e2023GL106062. https://doi.org/10.1029/2023GL106062

References From the Supporting Information

Eskes, H., & van Geffen, J. (2021). *Product user manual for the TM5 NO_2, SO_2 and HCHO profile auxiliary support product*. Tech. Rep. 1.0.0. KNMI. https://sentinel.esa.int/documents/247904/2474726/PUM-for-the-TM5-NO2-SO2-and-HCHO-profile-auxiliary-support-product.pdf/de18a67f-feca-1424-0195-756c5a3df8df

Gelaro, R., McCarty, W., Suárez, M. J., Todling, R., Molod, A., Takacs, L., et al. (2017). The modern-era retrospective analysis for research and applications, version 2 (MERRA-2). *Journal of Climate*, *30*(14), 5419–5454. https://doi.org/10.1175/JCLI-D-16-0758.1

Hoesly, R. M., Smith, S. J., Feng, L., Klimont, Z., Janssens-Maenhout, G., Pitkanen, T., et al. (2018). Historical (1750–2014) anthropogenic emissions of reactive gases and aerosols from the Community Emissions Data System (CEDS). *Geoscientific Model Development*, *11*(1), 369–408. https://doi.org/10.5194/gmd-11-369-2018

Lawrence, D. M., Oleson, K. W., Flanner, M. G., Thornton, P. E., Swenson, S. C., Lawrence, P. J., et al. (2011). Parameterization improvements and functional and structural advances in version 4 of the community land model. *Journal of Advances in Modeling Earth Systems*, *3*(1). https://doi.org/10.1029/2011MS00045

Mao, J., Jacob, D. J., Evans, M. J., Olson, J. R., Ren, X., Brune, W. H., et al. (2010). Chemistry of hydrogen oxide radicals (HO_x) in the Arctic troposphere in spring. *Atmospheric Chemistry and Physics*, *10*(13), 5823–5838. https://doi.org/10.5194/acp-10-5823-2010

Park, R. J., Jacob, D. J., Field, B. D., Yantosca, R. M., & Chin, M. (2004). Natural and transboundary pollution influences on sulfate-nitrate-ammonium aerosols in the United States: Implications for policy. *Journal of Geophysical Research*, *109*(D15), D15204. https://doi.org/10.1029/2003JD004473

van der Werf, G. R., Randerson, J. T., Giglio, L., van Leeuwen, T. T., Chen, Y., Rogers, B. M., et al. (2017). Global fire emissions estimates during 1997–2016. *Earth System Science Data*, *9*(2), 697–720. https://doi.org/10.5194/essd-9-697-2017